

NACA
SERVICE REPORT
RESEARCH MEMORANDUM

DECLASSIFIED:
ATS 480

AUTHORITY: for the
DROBKA TO LEBOW
MEMO DATED 12/13/65 U. S. Air Force

DRAG MEASUREMENTS ON EQUIVALENT BODIES OF REVOLUTION
OF SIX CONFIGURATIONS OF THE CONVAIR MX-1964
(ORIGINALLY MX-1626) PROPOSED

SUPERSONIC BOMBER

By James Rudyard Hall

Langley Aeronautical Laboratory
Langley Field, Va.

Declassified by authority of NASA
Classification Change Notices No. 43
Dated **12/22/65

CLASSIFICATION CHANGE TO CONFIDENTIAL
AUTHORITY: NASA RESEARCH ABSTRACTS
EFFECTIVE DATE: JANUARY 20, 1968

**NATIONAL ADVISORY COMMITTEE
FOR AERONAUTICS**

WASHINGTON

OCT 29 1953

RESEARCH MEMORANDUM

for the
U. S. Air Force**SERVICE REPORT**

DRAG MEASUREMENTS ON EQUIVALENT BODIES OF REVOLUTION

OF SIX CONFIGURATIONS OF THE CONVAIR MX-1964

(ORIGINALLY MX-1626) PROPOSED

SUPERSONIC BOMBER

By James Rudyard Hall

SUMMARY

Tests on equivalent bodies of revolution of six configurations of the Consolidated Vultee Aircraft Corporation proposed supersonic bomber (Convair MX-1964) have indicated that it is possible to reduce the drag of the configuration by designing it to have a favorable area distribution. The method of NACA RM L53I22c to predict the peak pressure drag of a configuration on the basis of its area distribution gave generally good agreement with the subject models.

INTRODUCTION

The recent promulgation of the transonic area rule (ref. 1) has produced widespread interest in the practicability of assessing the drag rise of a complete configuration by the use of a simple and inexpensive equivalent body of revolution. This extended application of the area rule has been substantiated in reference 2 for the type of configurations currently reported. The Langley Pilotless Aircraft Research Division of the NACA has tested six bodies of revolution of various configurations of the Consolidated Vultee Aircraft Corporation proposed supersonic bomber. The original configuration was known as the Convair MX-1626. Later versions were designated the Convair MX-1964. Two of these equivalent bodies were of configurations which had been previously tested. The remainder were tested to determine the effect on C_D of configuration modifications which changed the area distribution of the equivalent bodies.

[REDACTED]

The historical development of the tests is given below. The initial test was made of a 1/10-scale rocket model of the Convair MX-1626 (ref. 3). The high drag measured for the Convair MX-1626 was attributed to unfavorable area distribution and led to the design and testing by the NACA of a low-drag configuration incorporating a favorable area distribution. The drag of these two configurations was verified by equivalent body tests. Meanwhile the original configuration had been changed to incorporate a thicker and larger wing and four engines in underslung "siamese" pairs resulting in a very unfavorable area distribution. No equivalent body was flown of this configuration inasmuch as it would be expected to have drag at least as high as airplane configuration 1. In an effort to lower the high drag probably associated with this configuration, the effect of separating and staggering the nacelles was studied by testing a body of revolution having that area distribution.

At this point, as a result of an NACA-Air Force-Convair conference, a more systematic study of the effect of area distribution on configuration drag was undertaken utilizing three equivalent bodies of revolution, namely a "redesigned" version of the MX-1964 having separated staggered nacelles and incorporating favorable area distribution, an identical configuration with siamese underslung nacelles, and a shortened version of the former.

Results are presented of the drag of the six equivalent bodies tested between Mach numbers 0.8 and 1.3. The Reynolds number of the tests based on model length varied between 4.5×10^6 and 9.9×10^6 .

MODELS

The models tested were equivalent bodies of revolution of six configurations of the Consolidated Vultee Aircraft Corporation proposed supersonic bomber (Convair MX-1964). Three-view drawings of the configurations from which the models were derived are shown in figures 1 to 6. Also shown in each figure is the nondimensional area distribution of the complete configuration and its components, the nondimensional radius distribution of the equivalent body of revolution, and the Reynolds number range of each test. The models were constructed to conform to the radius distribution of each configuration after indenting the afterbody to compensate for the fin cross-sectional area. The scale of each model was chosen to give the equivalent body a maximum diameter of approximately 1.5 inches. The models are numbered 1 to 6 corresponding to the configurations of figure 1 to 6, respectively, and are shown in the photographs of figure 7.

Magnesium and aluminum construction were used entirely. The centers of gravity were located forward of 60 percent of the length to the fin-trailing-edge intercept. Measurements made on each model indicated that tolerances were held to ± 0.003 inch.

All the models except model 1 were of configurations having ducted nacelles. The nacelle area of open nacelle models was obtained by subtracting from the solid nacelle area a constant stream tube area equal to the entrance area times the mass flow ratio at Mach number 1.0. This procedure is verified for sharp-lipped inlets by the results of reference 5. Models 1 and 2 were previously tested and reported on in reference 3.

Configuration 1 was the Consolidated Vultee Aircraft Corporation MX-1626 with faired, solid nacelles and under-wing landing-gear fairings. Complete coordinates for this configuration are given in reference 3.

Configuration 2 was a configuration designed by the NACA to modify the MX-1626 to incorporate the principles of favorable area distribution. Aerodynamic considerations were given primary emphasis over problems such as balance, structure, and accessibility. If the principal aim of low drag was attained, it was felt that the lines could be revised to yield a workable airplane without compromising its area distribution. The design criterion for this configuration was the area distribution for a parabolic body of fineness ratio 9 with the maximum diameter at 50 percent of the length (see fig. 2). Reference 4 indicates this to be a low-drag body shape. Complete coordinates for this configuration are given in reference 3.

Configuration 3 was the Consolidated Vultee Aircraft Corporation proposed supersonic bomber MX-1964 with the nacelles separated and staggered. This configuration originally had underslung siamese nacelles with a resultant area distribution which was quite similar to that of the MX-1626 (configuration 1). An equivalent body of configuration 3 was tested to determine the benefit derivable from a separated and staggered nacelle installation.

Configuration 4 was a redesigned version of the MX-1964 designed to fit the area distribution of a parabolic body of fineness ratio 9 (see fig. 4). Changes from the original MX-1964 included lengthening and indenting the fuselage, separating and staggering the nacelles, and modifying the wing plan form from a delta wing to shallow diamond to utilize the slightly less abrupt rate of change of area at the rear portion of the wing. The airplane volume was held approximately constant throughout these changes.

Configuration 5 was exactly like configuration 4 except that the separated and staggered nacelles were replaced by a siamese installation.

CONFIDENTIAL

This model was flown in order to obtain the drag penalty associated with the substitution of siamese nacelles for split-staggered nacelles on a configuration which was otherwise identical.

Configuration 6 was like configuration 4 except that the fuselage was shortened in length from 1,125 inches to 1,075 inches. The alteration produced a slightly larger base and small change in the afterbody contour.

It should be noted at this point that subsequent wind-tunnel and rocket-model tests on area-rule versions of the MX-1964 will not be of configurations having the area distribution reported herein since some revisions have been made by CVAC in the original area distributions upon which the subject models were based.

The airplane wing areas corresponding to the test configurations are given in table I. Also given are the factors to convert the reported C_D (based on wing area) to C_D based on the maximum cross-sectional area of the body of revolution.

TESTS

The models were tested by firing them from the helium gun at the Langley Pilotless Aircraft Research Station, Wallops Island, Va. The gun is pictured in figure 8. In operation a model in a 6-inch-diameter sabot is placed in the breech of the gun. A push plate behind the sabot bears against it and the model. A cutaway photograph of the sabot assembly with a typical model, not connected with the present program, is shown in figure 9. A quick-opening valve admits helium to the gun barrel under about 200 pounds pressure accelerating the sabot assembly up the 23-foot-long barrel to supersonic velocities. Upon emerging from the barrel the three segments of the sabot and the push plate peel away and fall to earth within 50 yards. The model decelerates along a ballistic trajectory. In these tests a continuous velocity history was obtained by means of the Doppler velocimeter between Mach numbers of 1.3 and 0.8. The model flight path was obtained by integrating the velocity along a ballistic trajectory. Atmospheric conditions aloft were obtained by a radiosonde released at the time of the tests.

The model deceleration was computed from the velocity history and the coefficient of drag was computed from the relationship

$$C_D = - \frac{W}{gqS} (a + g \sin \gamma)$$

where W was the model weight, a was the model acceleration, g was acceleration of gravity, 32.2 ft/sec^2 , γ was flight path angle, S was reference wing area, and q was dynamic pressure.

The estimated accuracy of the measurements was as follows:

C_D	± 0.001
M	± 0.01

The Reynolds number of these tests was between 4.5×10^6 and 10×10^6 based on the length of the test models.

RESULTS AND DISCUSSION

Results of the drag measurements are presented in figures 1 to 6. A summary plot of drag coefficient C_D and drag-rise coefficient ΔC_D for all models tested is shown in figure 10. The drag-rise coefficient is defined herein as $(C_{D_{M=M}} - C_{D_{M=0.85}})$. The drag coefficients are based on the wing area of each configuration, although the comparative order of the curves would be the same if a constant wing area were used as the characteristic area.

The subject work is an extended application of the area rule of reference 1 which states that near the speed of sound the drag rise of a low-aspect-ratio, thin wing-body combination is primarily dependent on the axial distribution of the cross-sectional area. The applicability of the rule is supported by the test results of references 2 to 4.

In analyzing the distribution of area, use may be made of the results of reference 6 which indicates a parabolic body of fineness ratio 9 with the maximum diameter located at 50 to 60 percent of the length to have a low drag rise. Local departures from this should increase the drag more or less depending on the severity of the departure.

Analyzing the effect of model shape on the measured C_D for the current tests yields the following observations. Model 1 (fig. 1, MX-1626) had the most unfavorable area distribution due to the highly sloped forebody and afterbody and high peak area corresponding to a low overall fineness ratio of 6.7. Its unfavorable area distribution was reflected in the high pressure drag measured for the model. Conversely, model 2 (fig. 2) had a favorable area distribution approximating a parabolic body of fineness ratio 9. Its pressure drag was less than one-half that of model 1. The area distribution of model 3 (fig. 3, MX-1964 with split and staggered nacelles) was unfavorable mainly because



of the highly sloped afterbody resulting in high transonic drag rise. The effective bluntness of the afterbody is probably higher than the actual bluntness since the small protuberance at the rear would not be expected to affect the flow over the main afterbody ahead of it. The C_D of model 3 was less than model 1 but appreciably more than the low C_D measured for model 2. The high subsonic drag measured for models 1 and 3 indicates that separation of flow probably occurred at the blunt afterbody of these models leading to somewhat low drag-rise results. Model 4 exhibits a very favorable area distribution and a low drag rise. The effect of shortening and refairing the fuselage (model 6 compared with model 4) was within the accuracy of the measurements of C_D , indicating a possible advantage of the shorter airplane because of the weight saving. The use of siamese nacelles in model 5 in place of the separated, staggered arrangement of model 4 created a substantial departure from the area distribution of model 4 and induced a 50-percent increase in pressure drag. The high drag penalty associated with the siamese nacelle installation appears to reject it in favor of the split, staggered nacelle installation.

A small delay in drag-rise Mach number is evident for the models with the most favorable area distribution.

The C_D measured for models 2, 4, and 6 was very similar and almost entirely within the limits of accuracy of the measurements. Although these models represent approximations to parabolic bodies, the variation from a true parabolic body incurs a penalty in drag rise of about 40 percent as stated in reference 4. Figure 10(b) shows the drag rise reported in the foregoing reference for a parabolic body of revolution of fineness ratio 8.91 with the maximum diameter located at 60 percent of the length.

The method of reference 7 for predicting the drag of bodies on the basis of their area distribution gave generally good agreement with the test results. Figure 11 presents a line-of-agreement plot of predicted transonic drag rise against measured drag rise. Agreement is within 15 percent in every case except for model 3 which had lower drag than expected. The blunt afterbody of model 3 may explain why the prediction fails in this case. Note also that the predicted and measured ΔC_D of the parabolic body of reference 4 are in agreement.

CONCLUSIONS

Drag measurements were made on six bodies of revolution representing six configurations of the Consolidated Vultee Aircraft Corporation proposed supersonic bomber (Convair MX-1964). The following conclusions were drawn from the test results:

1. A favorable area distribution was necessary to achieve low zero-lift drag characteristics. Secondary improvements occurred in increased drag-rise Mach number.

2. The MX-1964 designed to incorporate the principles of good area distribution, the shortened version of this airplane and the NACA 4 nacelle configuration had similar transonic drag rises within the limits of accuracy of the measurements.

3. The use of separated, staggered nacelles on the original MX-1964 decreased the drag rise on the basis of that which would be expected from the previous test on the MX-1626. However, the drag level with split and staggered nacelles was excessively high compared with the results obtainable from a configuration incorporating a favorable area distribution.

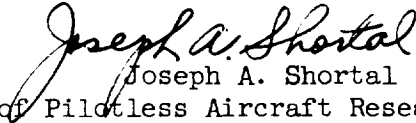
4. The method of NACA RM L53I22c for predicting the peak pressure drag of a configuration on the basis of its area distribution gave generally good agreement with the subject models.

Langley Aeronautical Laboratory,
National Advisory Committee for Aeronautics,
Langley Field, Va., October 19, 1953.



James Rudyard Hall
Aeronautical Research Scientist

Approved:



Joseph A. Shortal
Chief of Pilotless Aircraft Research Division

cg



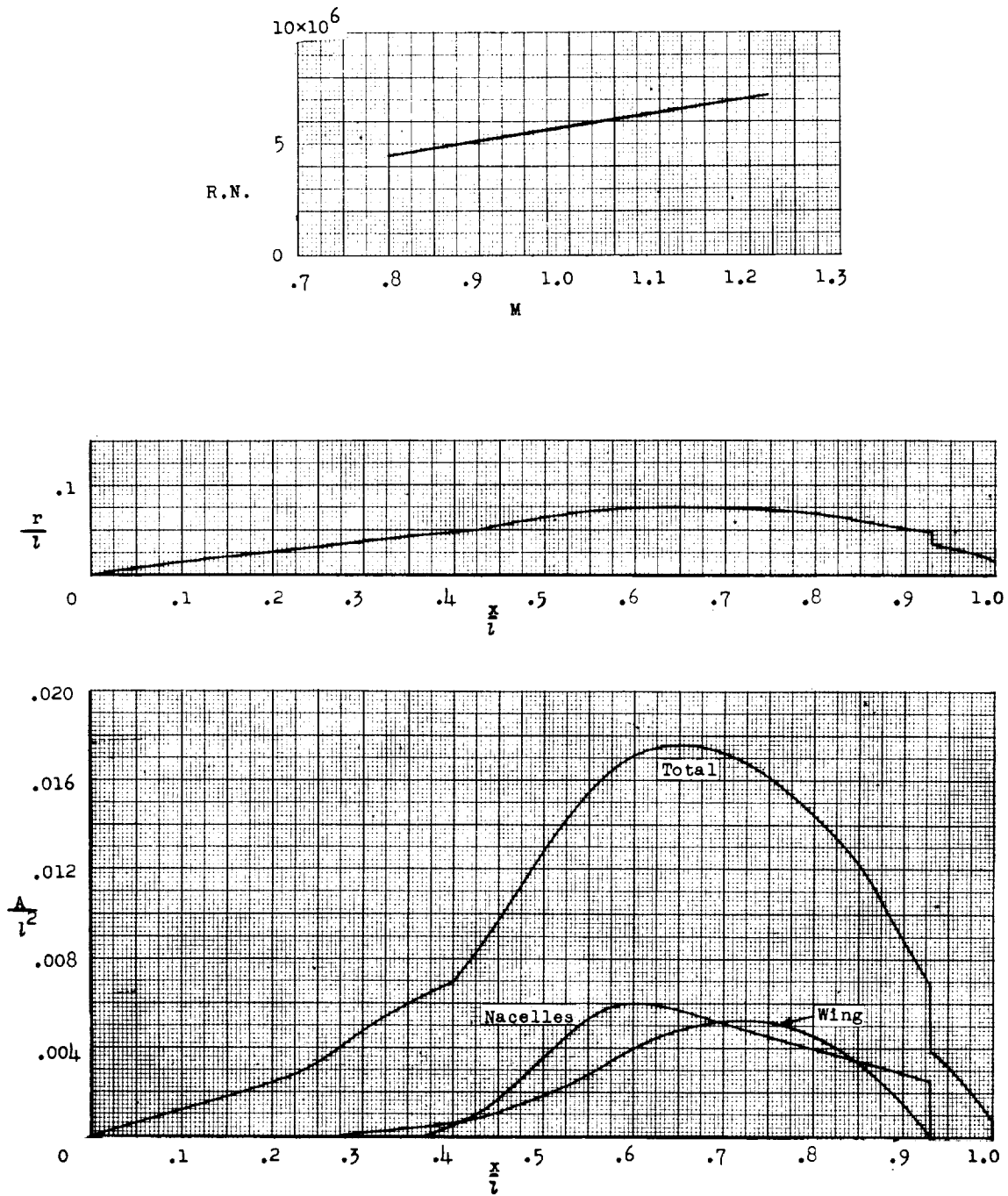
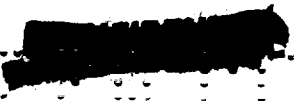
REFERENCES

1. Whitcomb, Richard T.: A Study of the Zero-Lift-Drag-Rise Characteristics of Wing-Body Combinations Near the Speeds of Sound. NACA RM L52H08, 1952.
2. Hall, James Rudyard: Comparison of Free-Flight Measurements of the Zero-Lift Drag Rise of Six Airplane Configurations and Their Equivalent Bodies of Revolution at Transonic Speeds. NACA RM L53J21a, 1953.
3. Hall, James R., and Hopko, Russell N.: Drag and Static Stability at Low Lift of Rocket-Powered Models of the Convair MX-1626 Airplane at Mach Numbers From 0.7 to 1.5. NACA RM SL53F09a, U. S. Air Force, 1953.
4. Hopko, Russell N., Piland, Robert O., and Hall, James R.: Drag Measurements at Low Lift of a Four-Nacelle Airplane Configuration Having a Longitudinal Distribution of Cross-Sectional Area Conducive to Low Transonic Drag Rise. NACA RM L52E29, 1953.
5. Walters, Richard E.: Application of Transonic Area Rule to a Sharp-Lipped Ducted Nacelles. NACA RM L53J09b, 1953.
6. Hart, Roger G., and Katz, Ellis R.: Flight Investigations at High-Subsonic, Transonic, and Supersonic Speeds To Determine Zero-Lift Drag of Fin-Stabilized Bodies of Revolution Having Fineness Ratios of 12.5, 8.91 and 6.04 and Varying Positions at Maximum Diameter. NACA RM L9I30, 1949.
7. Nelson, Robert L., and Stoney William E., Jr.: Pressure Drag of Bodies at Mach Numbers up to 2.0. NACA RM L53I22c, 1953.

CONFIDENTIAL

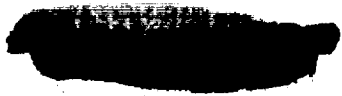
TABLE I

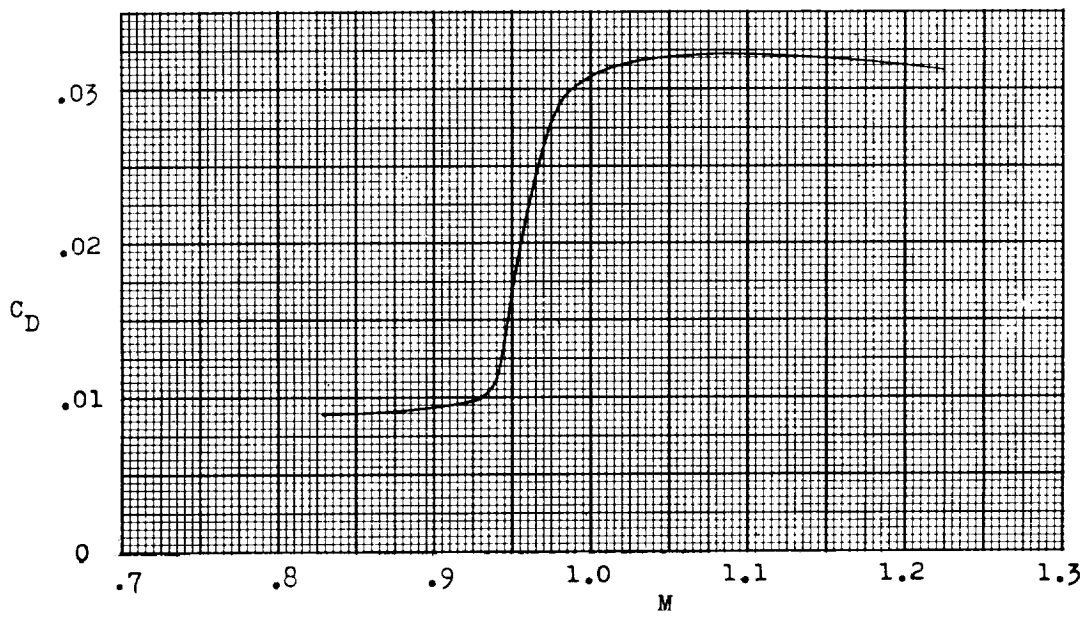
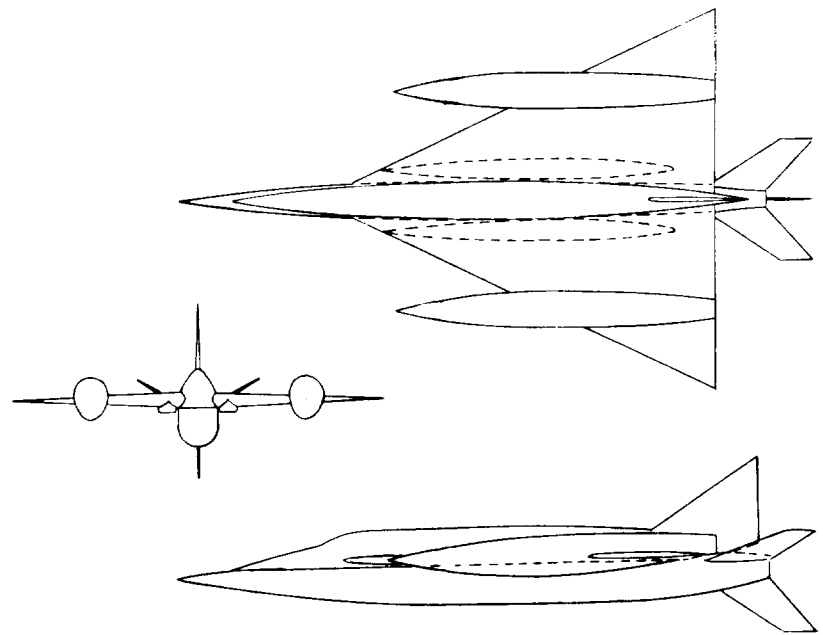
Model	Full-scale-airplane wing area, sq ft	Conversion factor for converting C_D based on wing area to C_D based on maximum cross-sectional area
1	1,200	12.2
2	1,542	18.2
3	1,400	14.3
4	1,542	17.9
5	1,542	15.2
6	1,542	17.9



(a) Nondimensional area and radius distribution and Reynolds number range of the test.

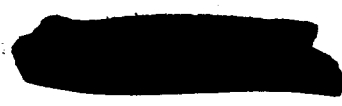
Figure 1.- Physical characteristics of model 1 and test results.

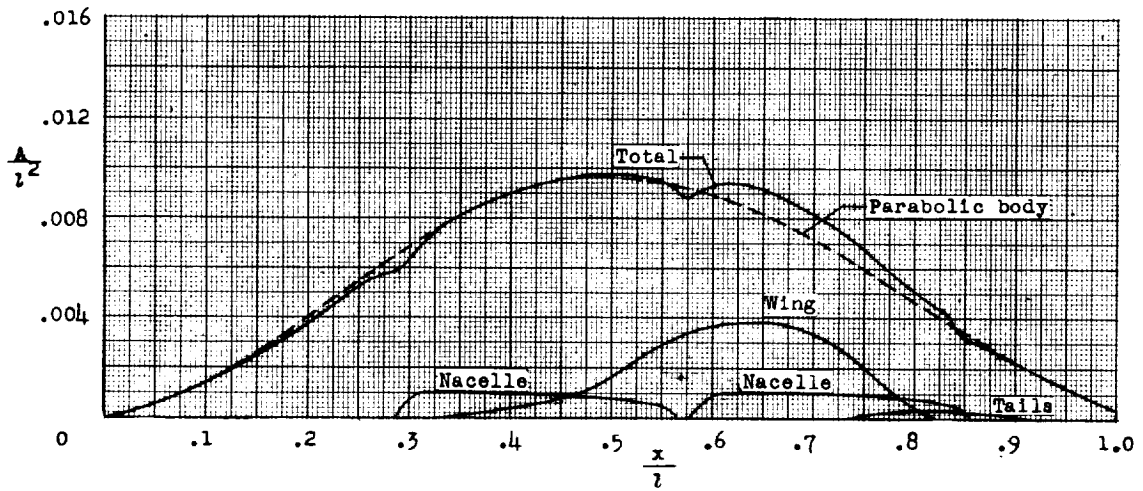
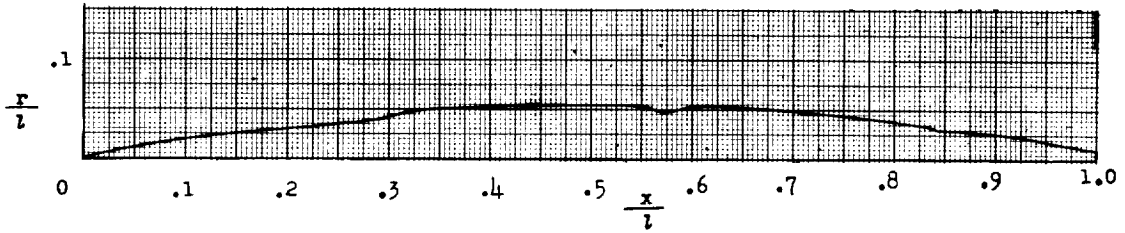
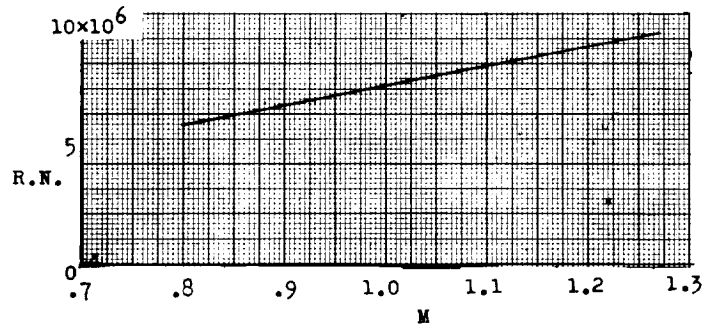




(b) General arrangement of configuration 1 and C_D of body of revolution 1 based on wing area of configuration 1.

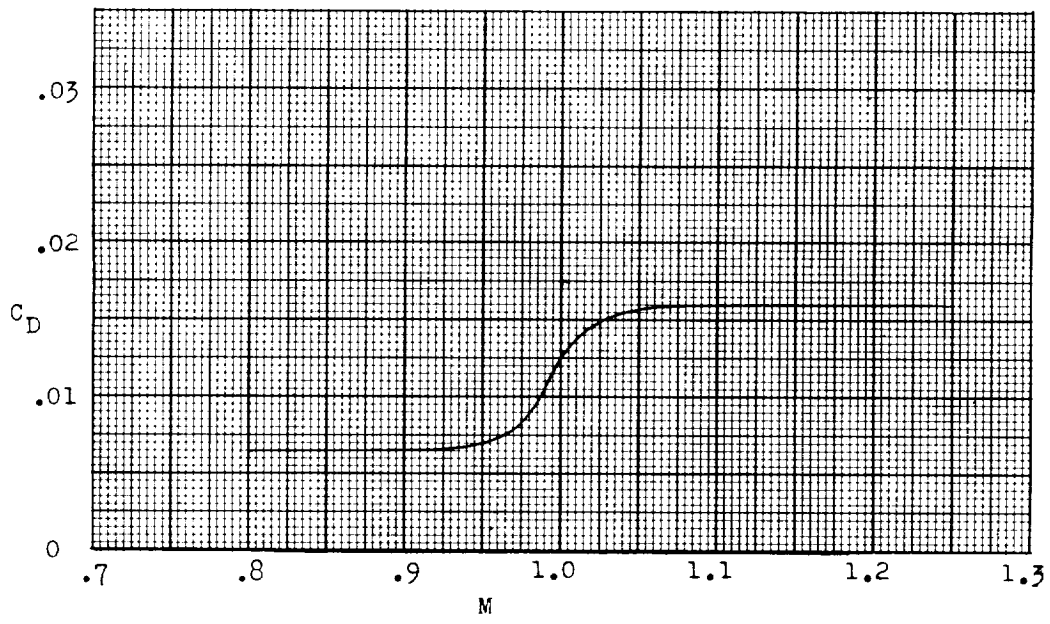
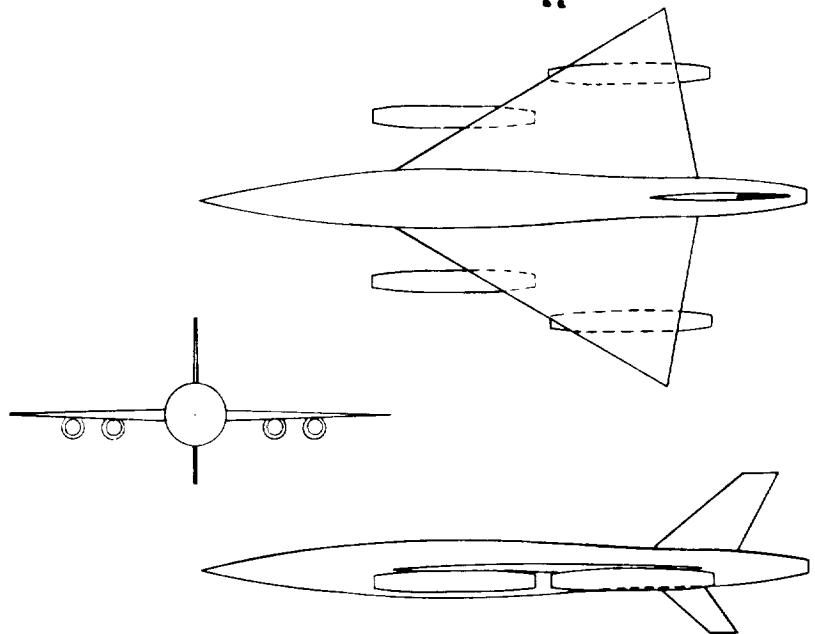
Figure 1.- Concluded.





(a) Nondimensional area and radius distributions and Reynolds number range of test.

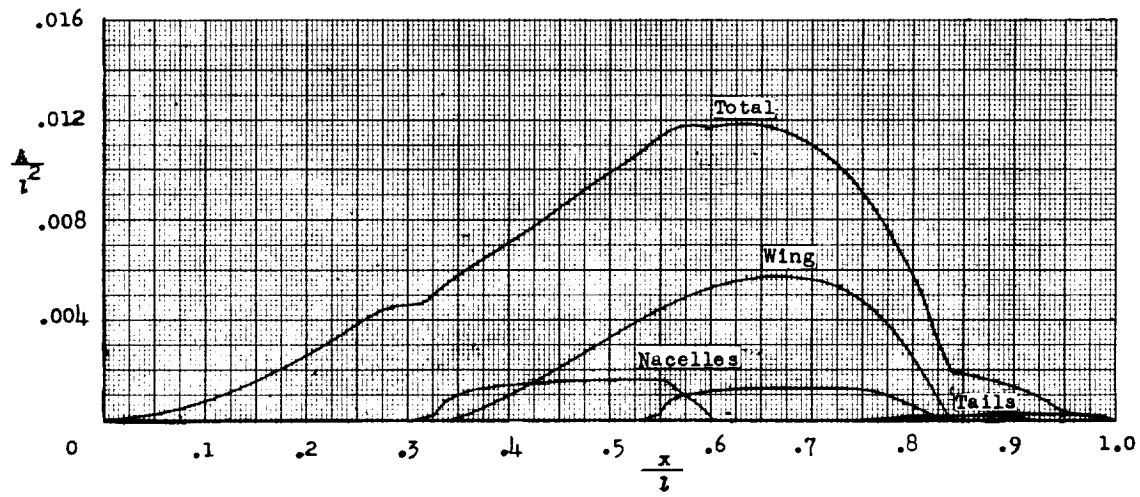
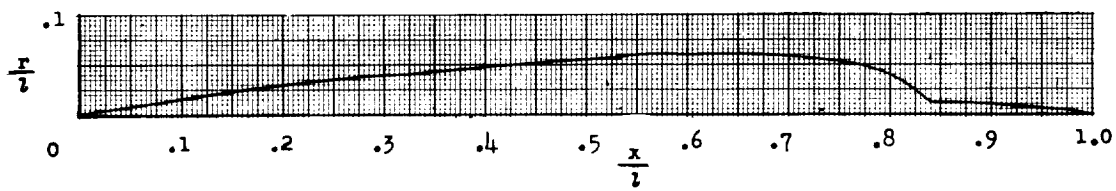
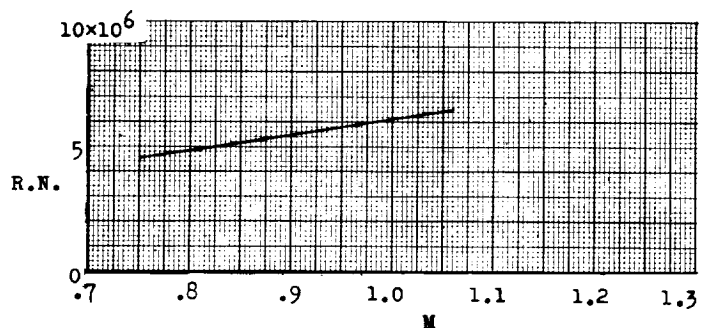
Figure 2.- Physical characteristics of model 2 and test results.



(b) General arrangement of configuration 2 and C_D of body of revolution 2 based on wing area of configuration 2.

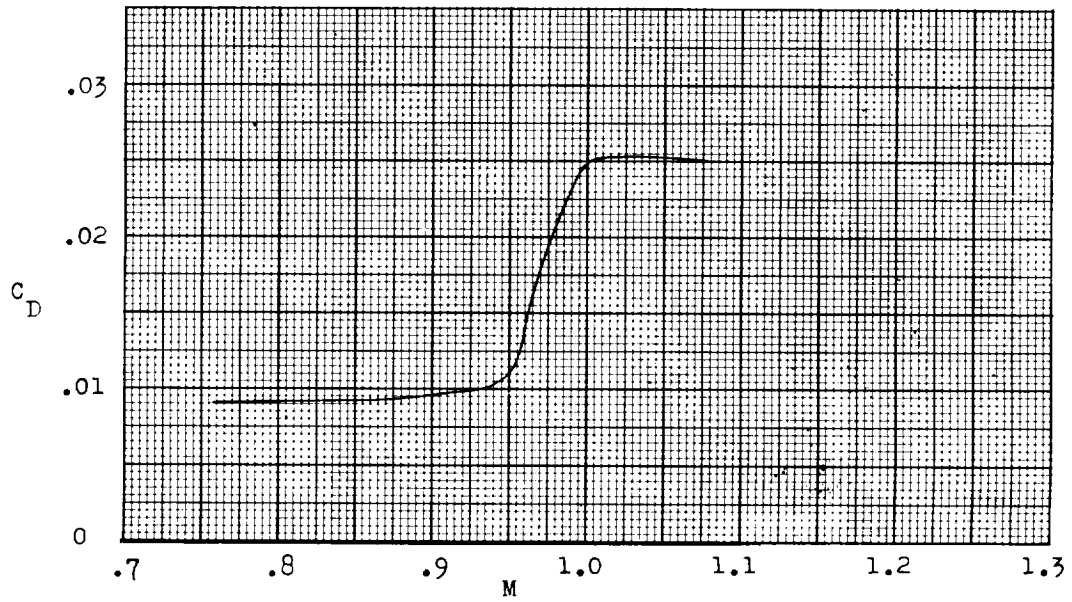
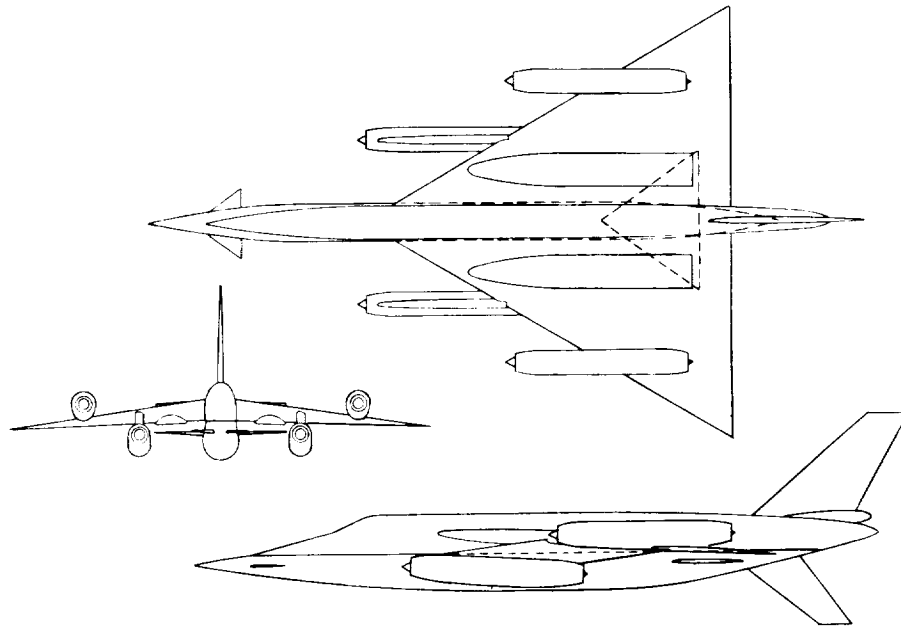
Figure 2.- Concluded.





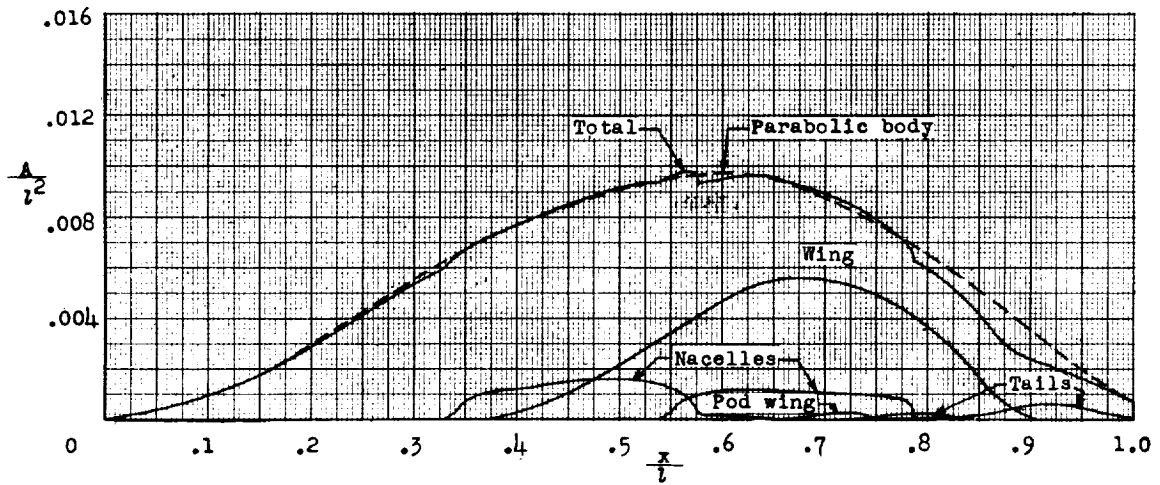
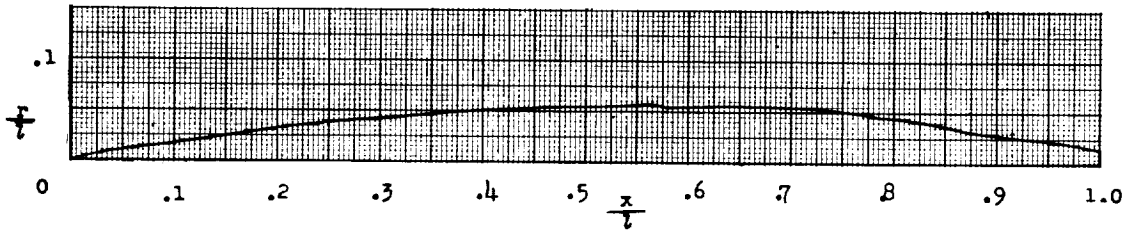
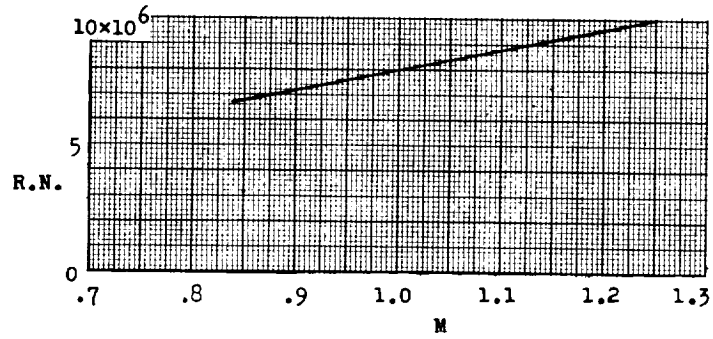
(a) Nondimensional area and radius distributions and Reynolds number range of test.

Figure 3.- Physical characteristics of model 3 and test results.



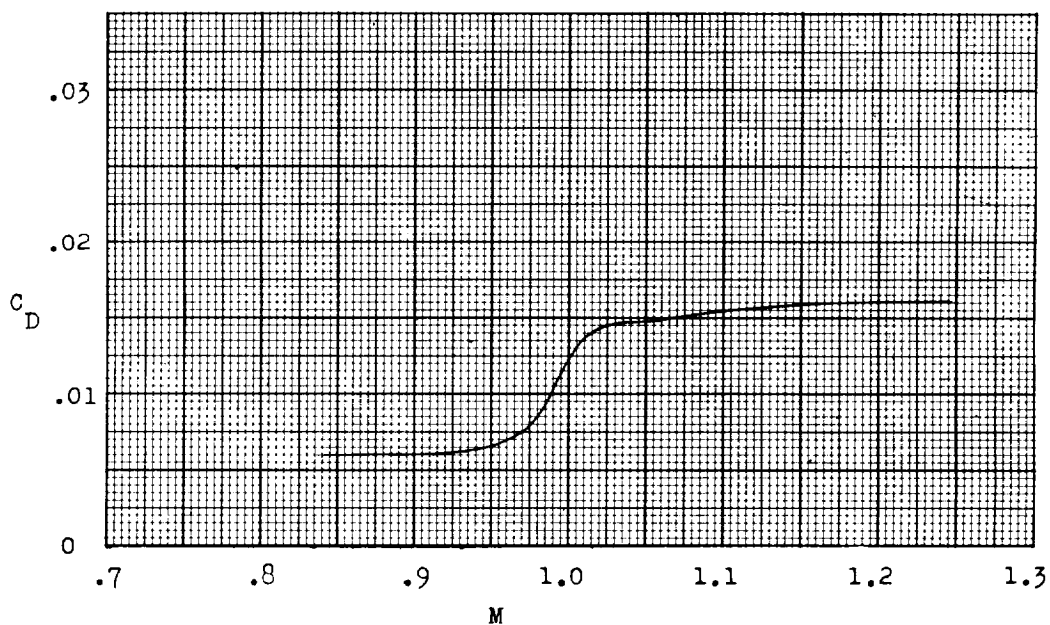
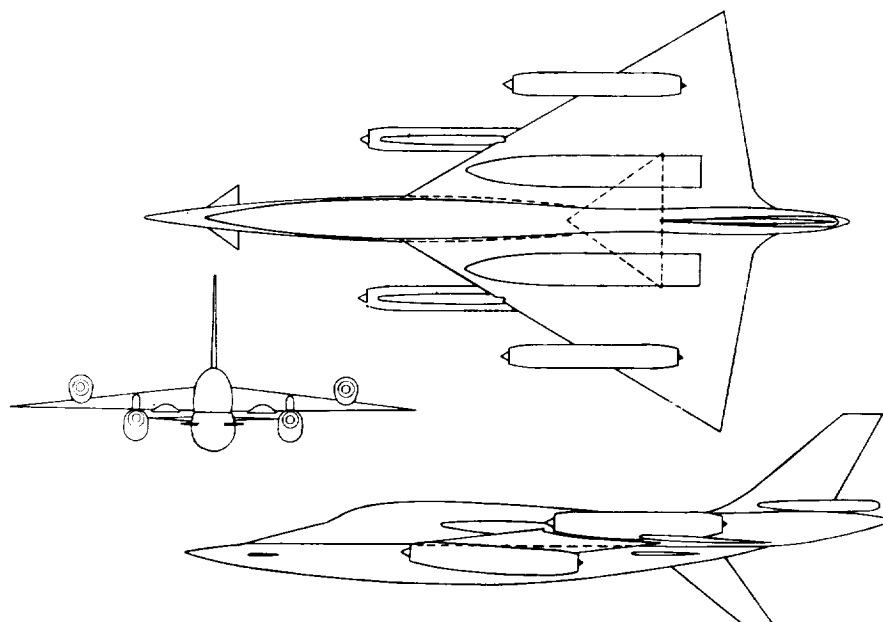
(b) General arrangement of configuration 3 and C_D of body of revolution 3 based on wing area of configuration 3.

Figure 3.- Concluded.



(a) Nondimensional area and radius distributions and Reynolds number range of test.

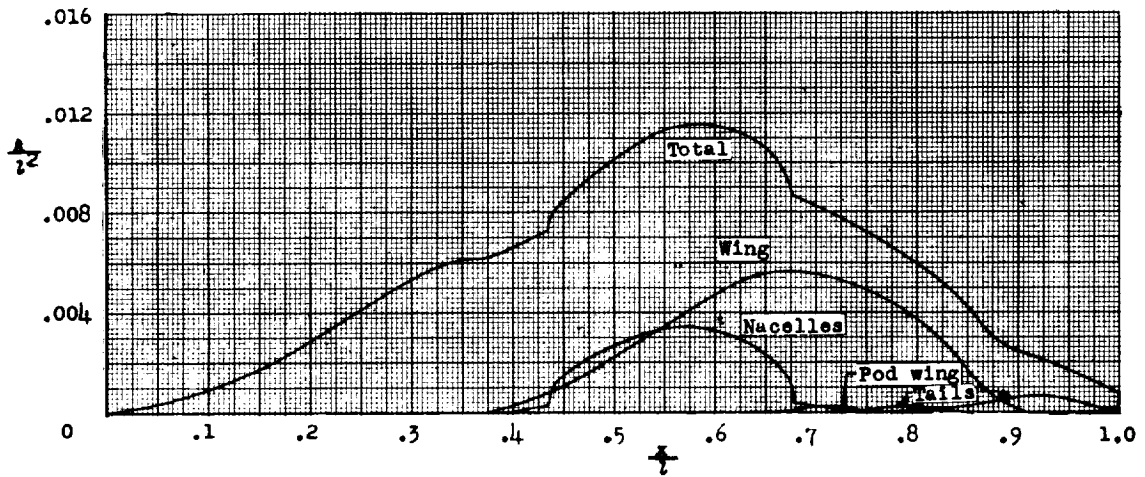
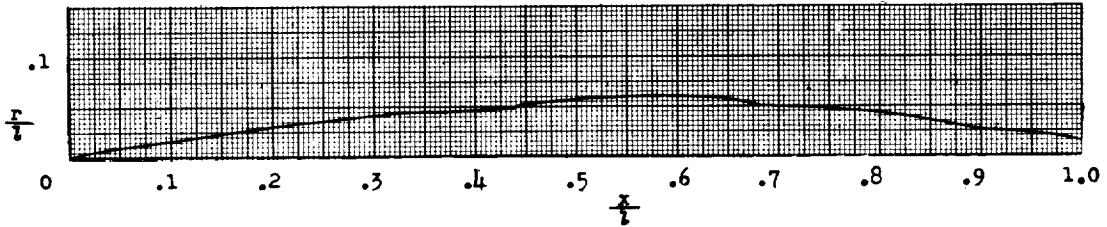
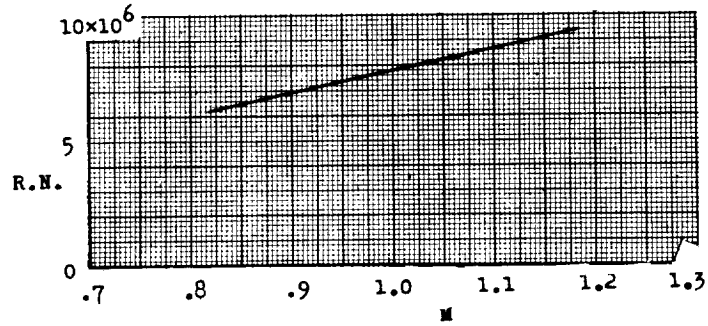
Figure 4.- Physical characteristics of model 4 and test results.



(b) General arrangement of configuration 4 and C_D of body of revolution 4 based on wing area of configuration 4.

Figure 4.- Concluded.

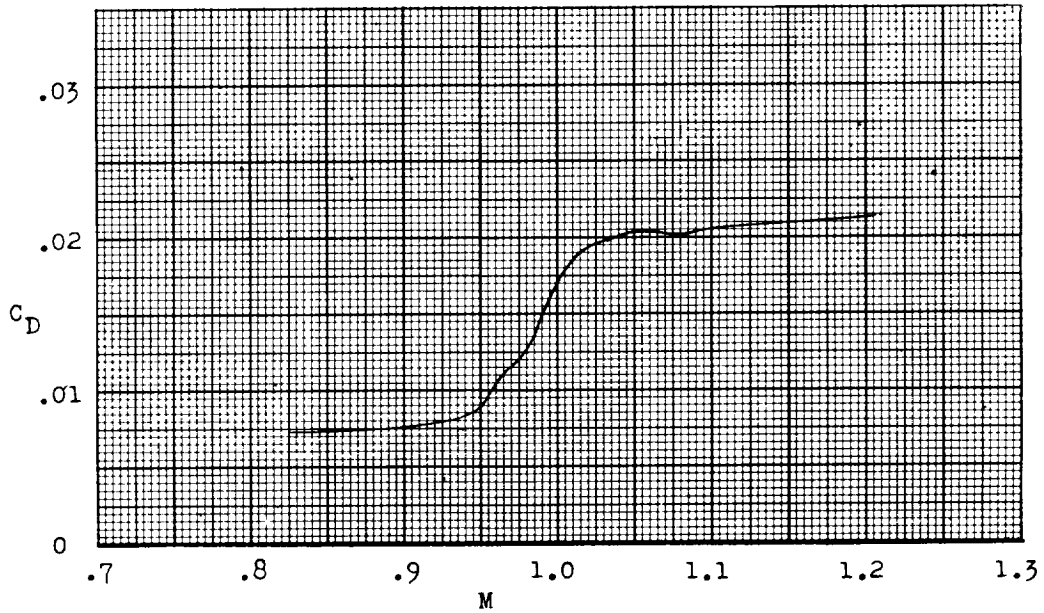
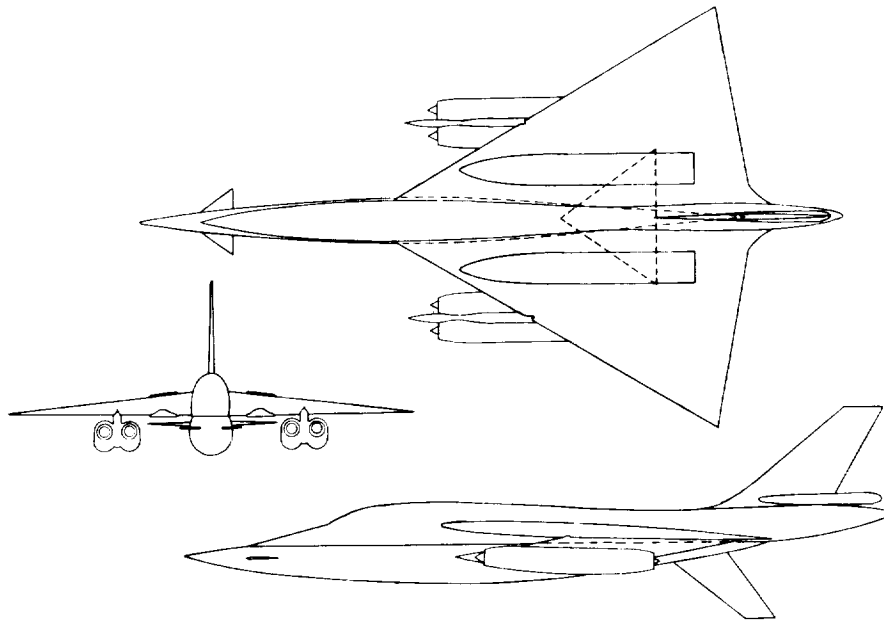
CONFIDENTIAL



(a) Nondimensional area and radius distributions and Reynolds number range of test.

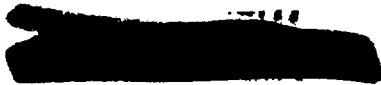
Figure 5.- Physical characteristics of model 5 and test results.

CONFIDENTIAL

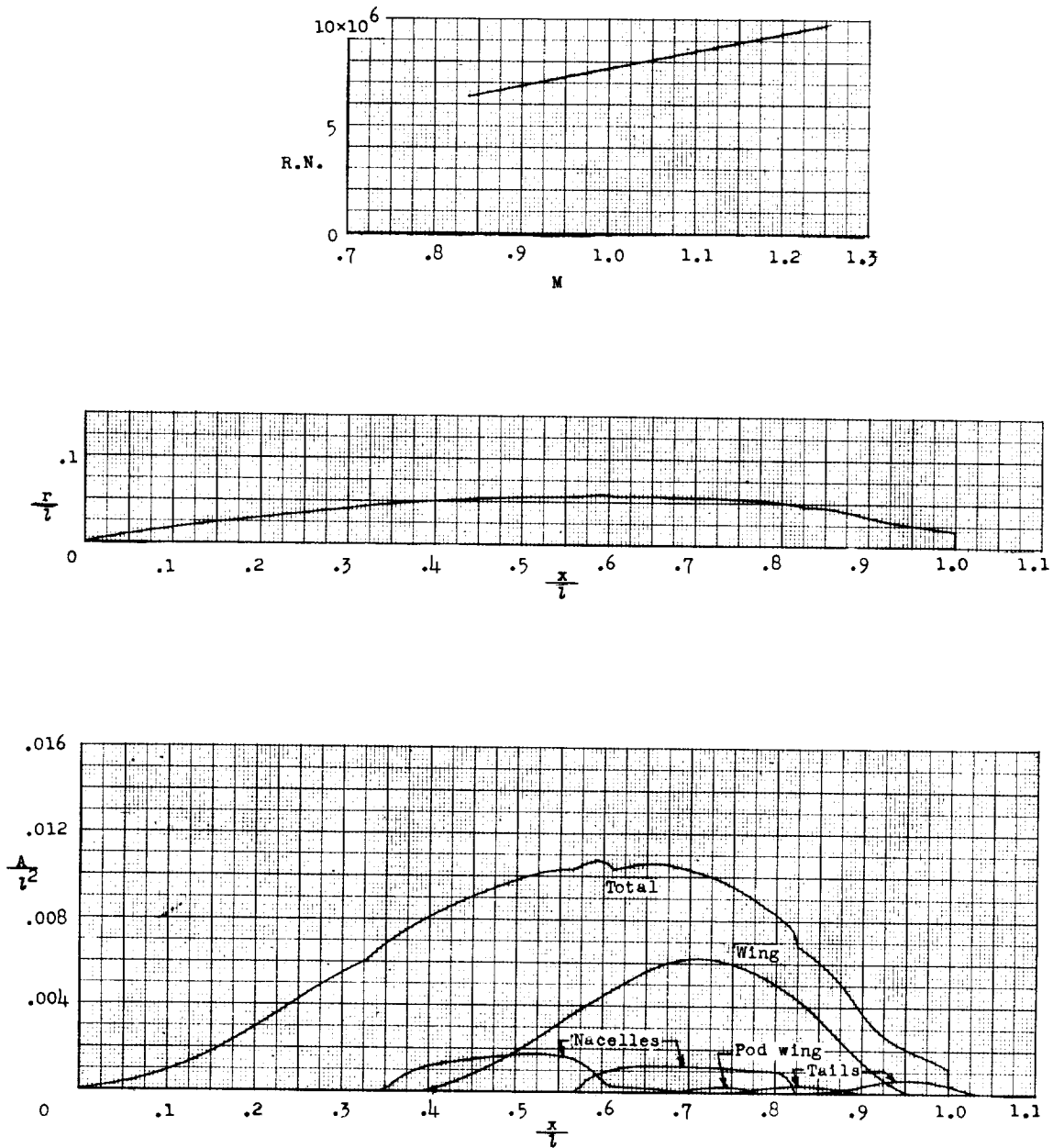


(b) General arrangement of configuration 5 and C_D of body of revolution 5 based on wing area of configuration 5.

Figure 5.- Concluded.



CONFIDENTIAL

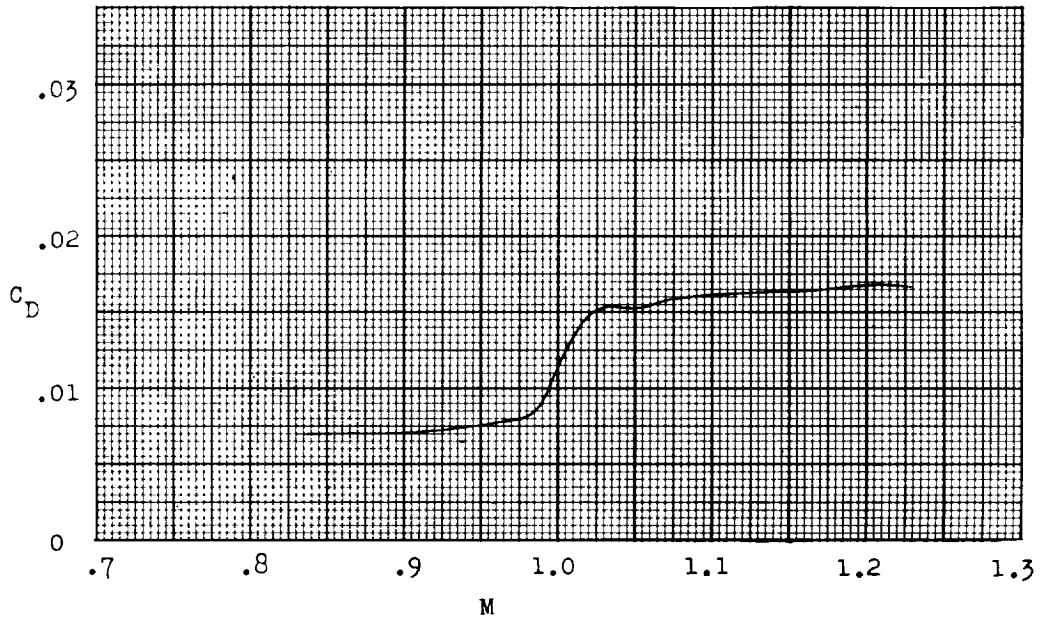
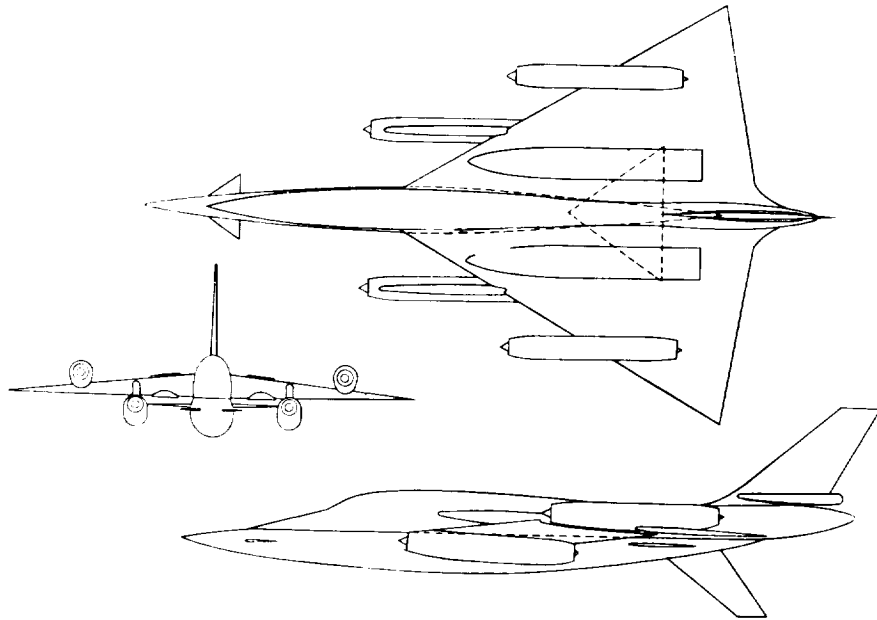


(a) Nondimensional area and radius distributions and Reynolds number range of test.

Figure 6.- Physical characteristics of model 6 and test results.

CONFIDENTIAL

CONFIDENTIAL



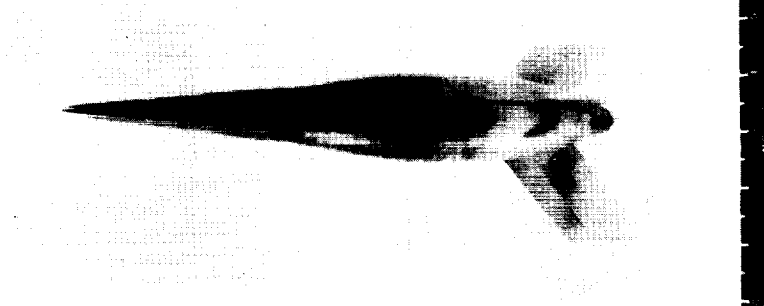
(b) General arrangement of configuration 6 and C_D of body of revolution 6 based on wing area of configuration 6.

Figure 6.- Concluded.

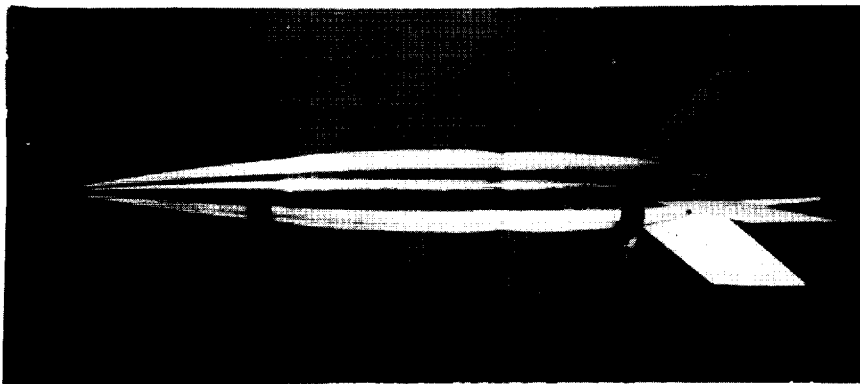


~~CONFIDENTIAL~~

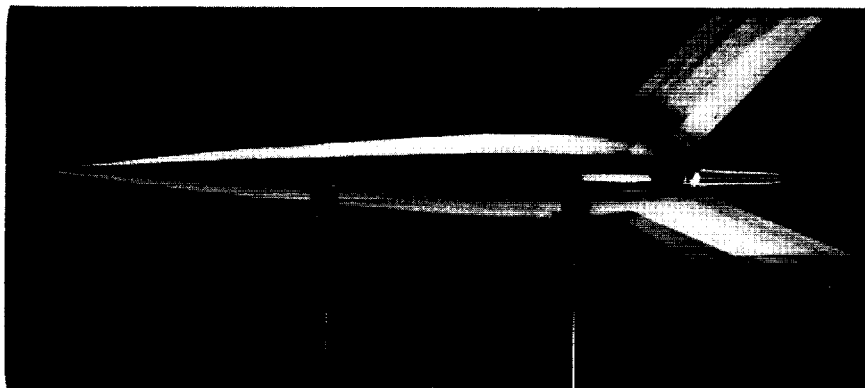
CONFIDENTIAL



(a) Model 1.



(b) Model 2.



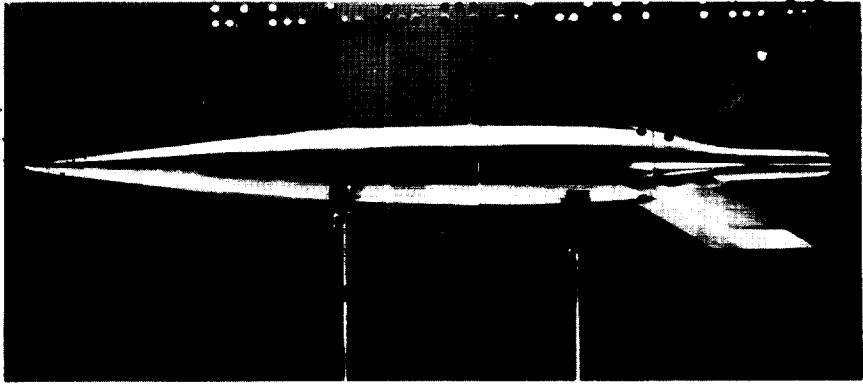
(c) Model 3.

L-82023

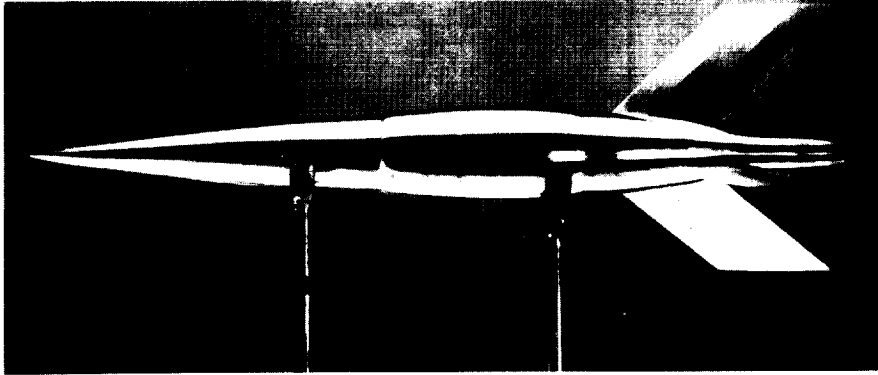
Figure 7.- Photographs of the test models. Model 1 was photographed standing on its fin tips and is shown horizontal to be consistent with the others.

~~CONFIDENTIAL~~

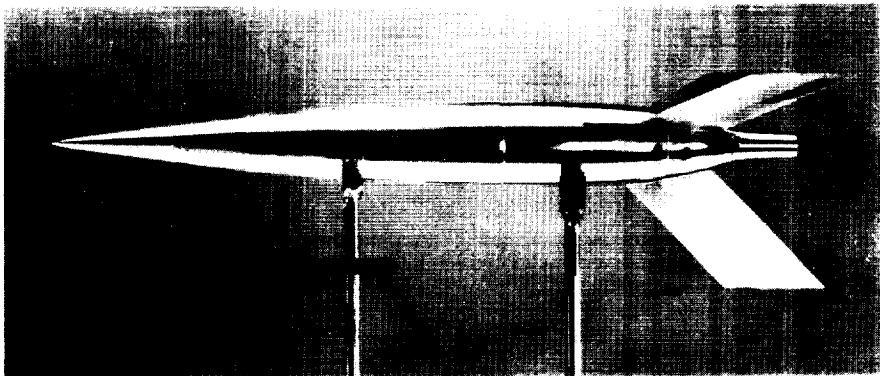
[REDACTED]
[REDACTED]



(d) Model 4.



(e) Model 5.

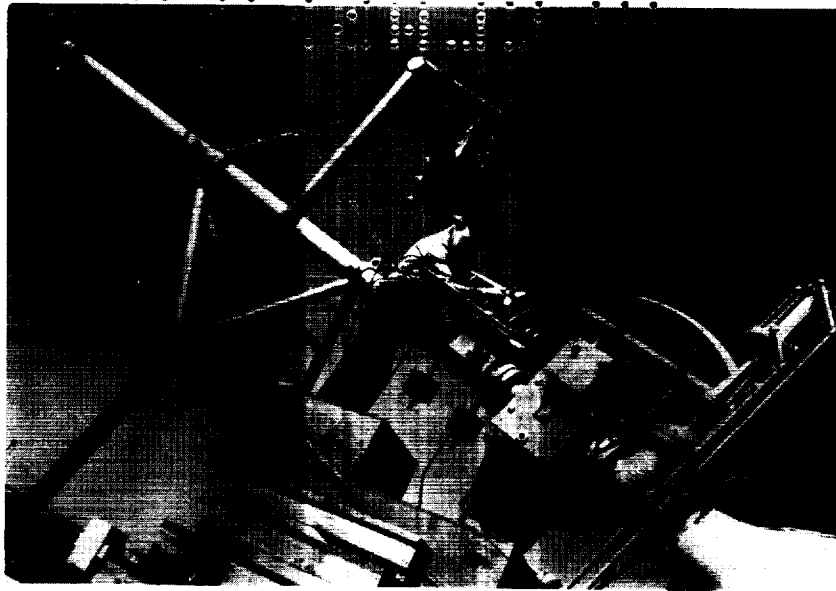


(f) Model 6.

L-82024

Figure **[REDACTED]** Concluded

[REDACTED]



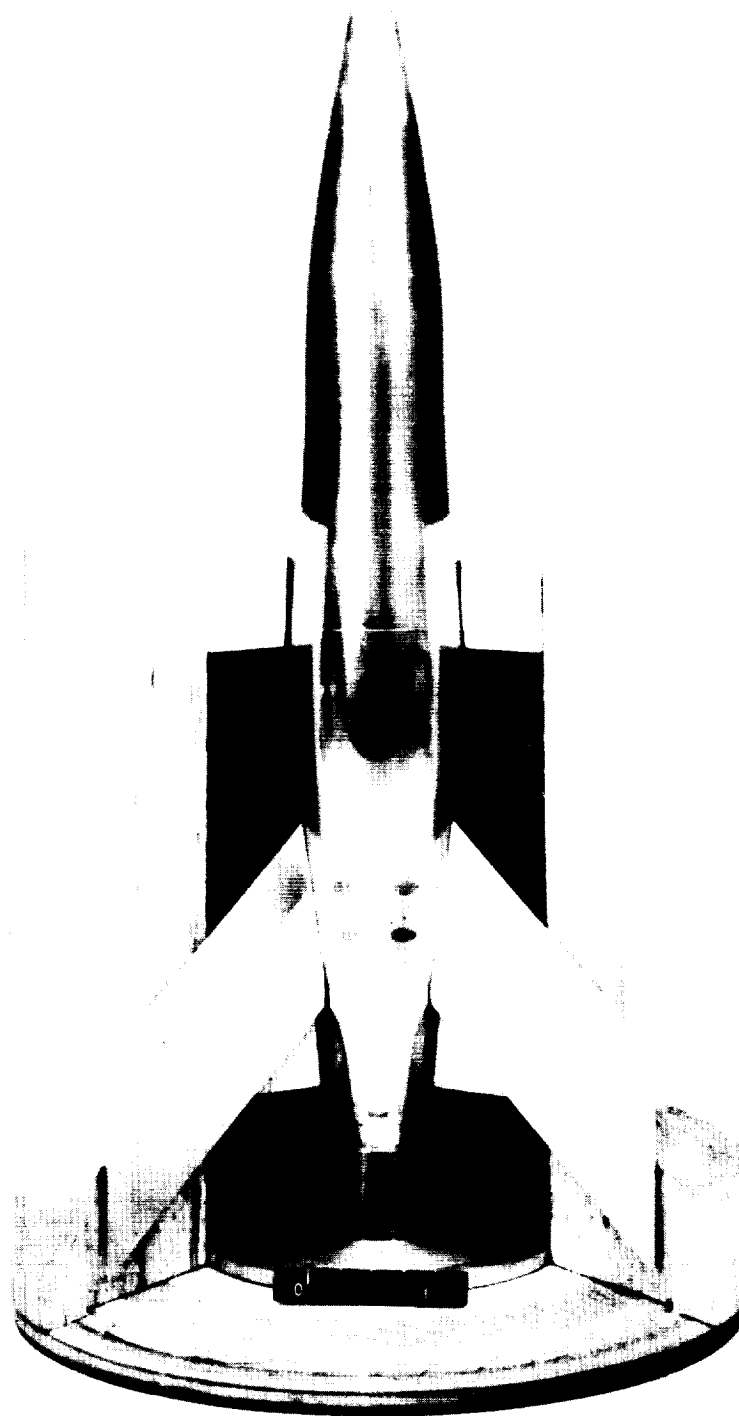
(a) Model being placed in helium gun. L-71457



(b) General arrangement showing helium supply tank, quick-opening valve mechanism, barrel and barrel truss, and Doppler velocimeter used to track model. L-66870

Figure 8.- Photographs of helium gun.

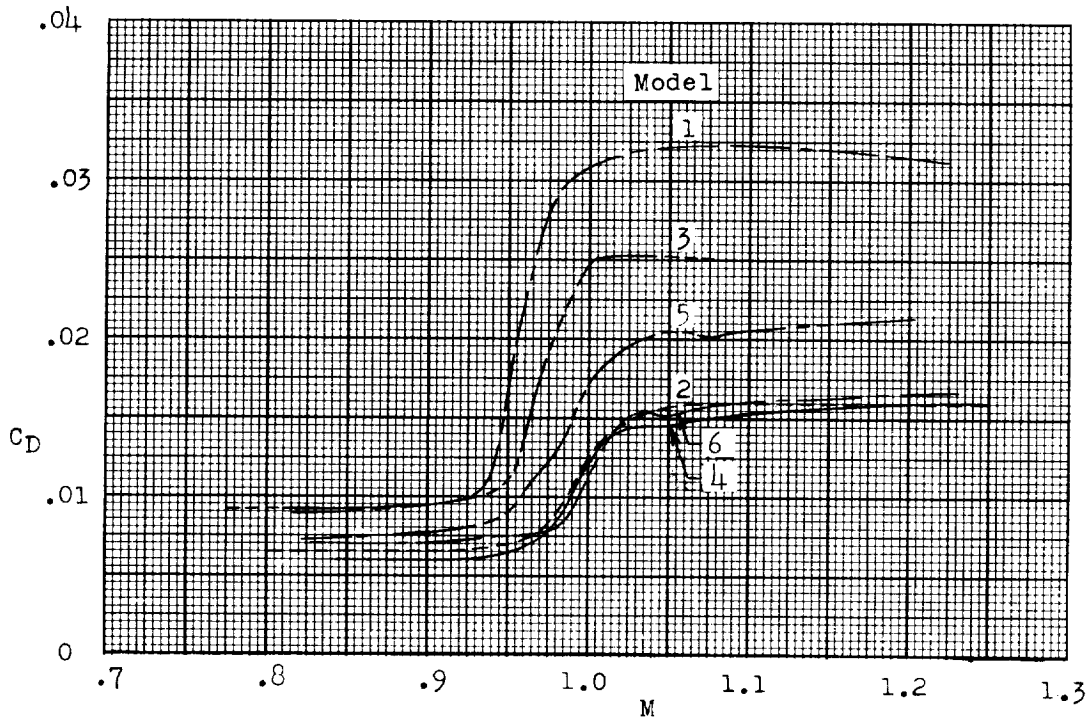




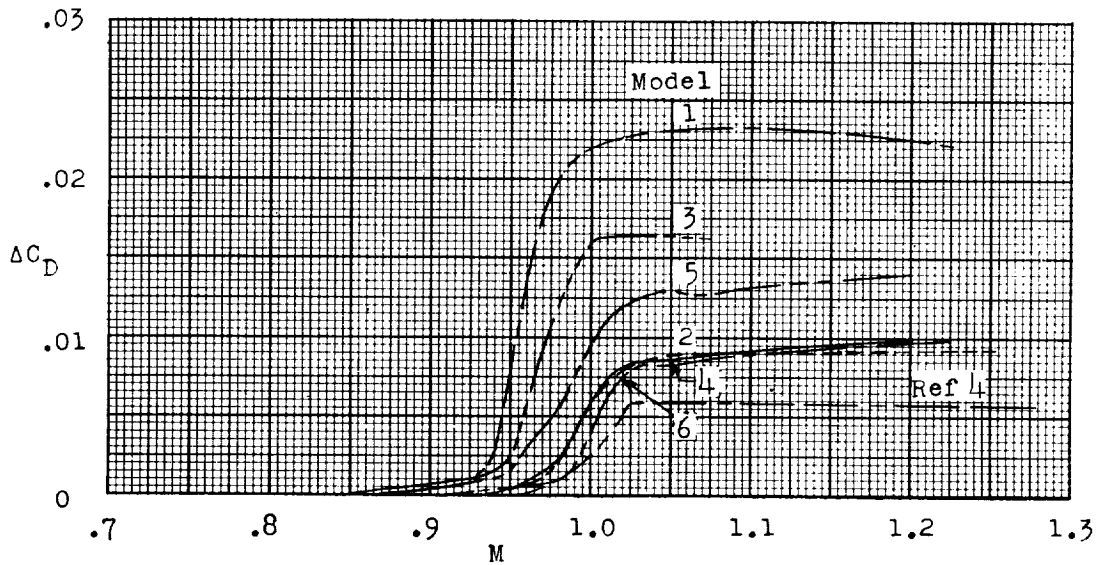
L-79811

Figure 9.- Cutaway photograph of typical model mounted in sabot.





(a) Drag coefficient of test models.



(b) Pressure drag of test models.

Figure 10.- Summary plots of test results.

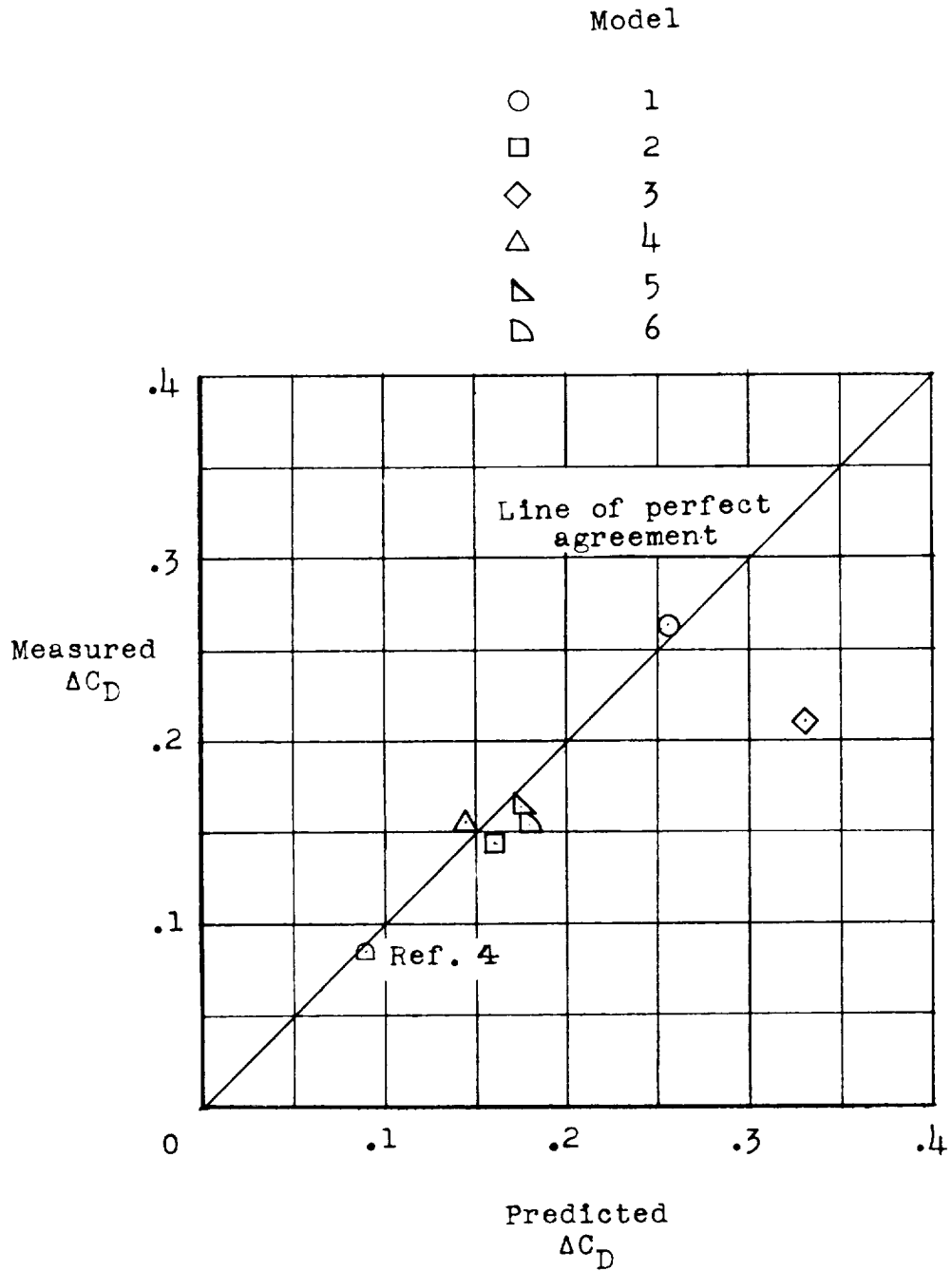


Figure 11.- Comparison of measured pressure drag coefficient and predicted pressure drag coefficient based on frontal area.

[REDACTED]

[REDACTED]